Improving the Microstructure and Mechanical Properties of Laser Welded Al-Si Coated 22MnB5/ Galvanized Steel Joint Added by Nickel

Youping Zhang , Youqiong Qin * , Feng Zhao , Min Liang

Posted Date: 21 July 2023

doi: 10.20944/preprints202307.1453.v1

Keywords: Laser welding; Al-Si coated hot stamping steel; Galvanized steel; Microstructure; Mechanical properties; Ni foil

Article

Improving the Microstructure and Mechanical Properties of Laser Welded Al-Si Coated 22MnB5/ Galvanized Steel Joint Added by Nickel

Youping Zhang, Youqiong Qin *, Feng Zhao and Min Liang

School of Material Engineering, Shanghai University of Engineering Science, Shanghai 201620, PR China
* Correspondence: E-mail:qyqqin@163.com

Abstract: To weaken the harm of Al-Si coating and increase the strength of welded joint, variable thickness of Ni foil (Ni, an austenitic formation element) was added into the lap laser welding Al-Si coated 22MnB5 hot stamping steel/galvanized steel joints. The joints' weld appearance, microstructure, and mechanical properties were explored. The weld altered from X-shape to Y-shape with the increased thickness of Ni foil. During welding, Al-Si coating was melted and diluted into the welding pool, forming δ-ferrite (a rich-Al phase with low toughness and strength) in FZ and FB. This phase deteriorated the strength of the joints. After adding Ni, the amount and size of the δ-ferrite phase decreased. With a significant thickness of Ni foil, δ-ferrite would disappear. However, a new phase (FM, rich-Ni phase) probably formed except PM(a no or negligible Ni phase). The heat-affected zone (HAZ) on the side of 22MnB5 comprised a coarse martensite zone, refined martensite zone, martensite+ferrite zone, and tempered martensite zone from the FZ to the basic material. HAZ on the side of galvanized steel mainly contained ferrite and pearlite. After adding Ni foil, the strength of the joint was more than that without Ni. The maximum strength of the joint can be up to 679MPa because of the disappearance of δ-ferrite. Meanwhile, the toughness of the joint increased. The fracture mode was from three mixed fractures(cleavage, quasi-cleavage, and dimple) to one fracture(dimple).

Keywords: laser welding; Al-Si coated hot stamping steel; galvanized steel; microstructure; mechanical properties; Ni foil

1. Introduction

The increasing popularity of automotive lightweight design concepts has greatly promoted the application and extensively of ultra-high strength steels (UHSS) [1–3]. 22MnB5 steel is an ordinary steel with an ultimate tensile strength of 1.5GPa after hot stamping. During the hot stamping process, 22MnB5 steel was heated to 900~950 °C, held for 5-10 minutes, and then stamped and quenched in a closed and water-cooled mold to obtain full-martensite[4]. However, there are some problems in the hot stamping process, such as oxidation and decarburization on the surface of the steel. The coating was a highly effective method of protecting the steel. A robust barrier was Al-Si coating, which was often utilized to solve problems and had a thickness of 20-40μm [5,6].

In the extensive application of Al-Si coated 22MnB5 hot stamping steel, it was possible to meet some problems of joining 22MnB5 to conventional steel (such as galvanized steel). To be strange, the serious problem was a new phase formed in fusion zone(FZ) or fusion boundary (FB) which decreased the mechanical properties of the welded joint during the lasing welding of Al-Si coated 22MnB5 by itself or dissimilar steels between Al-Si coated 22MnB5 and conventional steel. The reason is: Al-Si coating melted and entered into the molten pool during the welding process. In the following cooling process, Al was aggregated in the FZ or FB, accordingly Al-rich phase formed in the FZ or FB. The crack often originated and extended from this phase [7–9].

Preprints (www.preprints.org) | NOT PEER-REVIEWED | Posted: 21 July 2023 doi:10.20944/preprints202307.1453.v1

For the studying of the aluminum-rich phase, different researchers had their different results. Kim et al. [10] considered the aluminum-rich phase as Fe-Al brittle intermetallic compounds (IMC) which weakened the strength of the joint. However, Other researchers revised the result. Because only Al was up to 12wt.% in Fe-Al binary phase diagram, Fe-Al intermetallic compounds are probably produced. Therefore, the opinion was that the aluminum-rich phase was δ-ferrite. Al is a ferrite-stabilizing element. Al-Si coating diluted in the welding pool and aggregated, which promoted a high-temperature phase forming. Lin et al. [11] considered the Al-rich phase was not Fe-Al intermetallic compound. Saha et.al. [12] also confirmed that the phase was δ-ferrite through the phase diagram. The hardness of Al-rich phase was very low which was a soft phase.

Based on the above, the traditional method was to remove the Al-Si coating before welding, such as laser cleaning and sandpaper grinding. But the additional work would consume time and increase the cost. Therefore, in-situ ablation methods were used and studied in laser welding Al-Si coated hot stamping steel. Lin et al. [13] provided a laser filler welding (a low carbon steel filler metal added). Through the dilution effect of filler wire and the enhancement of the flow of the molten pool, the content and distribution of δ-ferrite decreased which improved the mechanical properties of the welded joint. VÖLKERS et al. [14] applied an ultrasonic coupled laser welding to inhibit the Al segregation in the fusion zone. Khan et al. [15] depressed the formation of δ-ferrite by coating colloidal graphite on the surface of 22MnB5 steel to reduce the concentration of δ-ferrite. In this study, an autenite-stabilizing element, Ni was added to the alloy of molten pool. A Variable thickness of Ni foil was added between the two base materials. The microstructure and mechanical properties of welded joints under different Ni foil thicknesses were studied.

2. Experimental materials and procedures

In this study, the experimental materials were 1.4mm thick Al-Si coated 22MnB5 hot-stamping steel and 2mm thick DC51D hot-dip galvanized steel. The microstructure of the base materials is shown in Figure 1. The microstructure of 22MnB5 steel was martensite, and the microstructure of galvanized steel (GA) was ferrite (F) and a small amount of pearlite (P). The chemical composition and tensile properties of the two base materials are shown in Table 1. The ultimate tensile strength (UTS) and yield strength (YS) of 22MnB5 steel were 1500MPa and 1200MPa, respectively. Galvanized steel (GA) had an ultimate tensile strength (UTS) and yield strength (YS) of 350MPa and 300MPa, respectively, and an elongation of 11.5%.

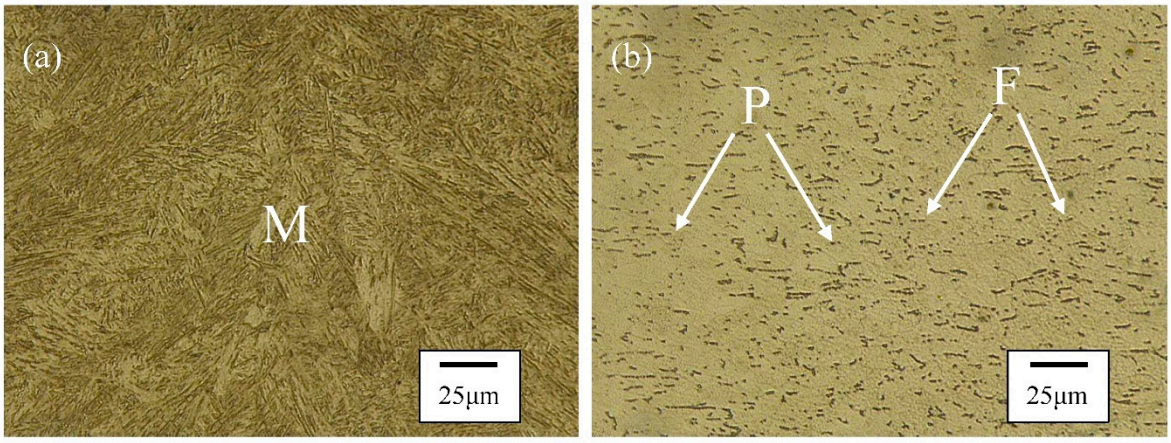

Figure 1. Microstructure of 22MnB5 steel (a) and galvanized steel (b) (M:martensite; P:pearlite; F:ferrite).

Table 1. Chemical compositions (wt.%) and tensile properties of base materials.

	Chemical compositions (w.%)								Tensile properties		
BM	C	Mn	Si	Cr	B	Ti	Al	Fe	UTS (MPa)	YS (MPa)	Elongations (%)
22MnB5	0.23	1.13	0.27	0.16	0.0025	0.038	0.037	Bal	1500	1200	4.1

Preprints (www.preprints.org) | NOT PEER-REVIEWED | Posted: 21 July 2023 doi:10.20944/preprints202307.1453.v1

GA steel	0.041	0.187	0.018	0.04	—	0.011	0.0032	Bal	350	300	11.5

The Al-Si coating thickness of 22MnB5 steel is about 30μm, and the coating thickness of galvanized steel is about 10μm. The Al-Si coating consists of α-Fe (Al, Si), $Fe_2(Al, Si)_5$ and Fe(Al, Si), named I, II and III zones in Figure 2a, samed as references [16,17]. For the GA coating, it is primarily composed of two regions, Region IV was $Fe_3Zn10(\Gamma)$, $Fe_5Zn_{21}(\Gamma_1)$, and region V was $FeZn_{10}$ (δ), $FeZn_{13}(\zeta)$ as shown in Figure 2b, samed as references [18,19]. All sheets are machined into 100mm×80mm sizes by wire EDM.

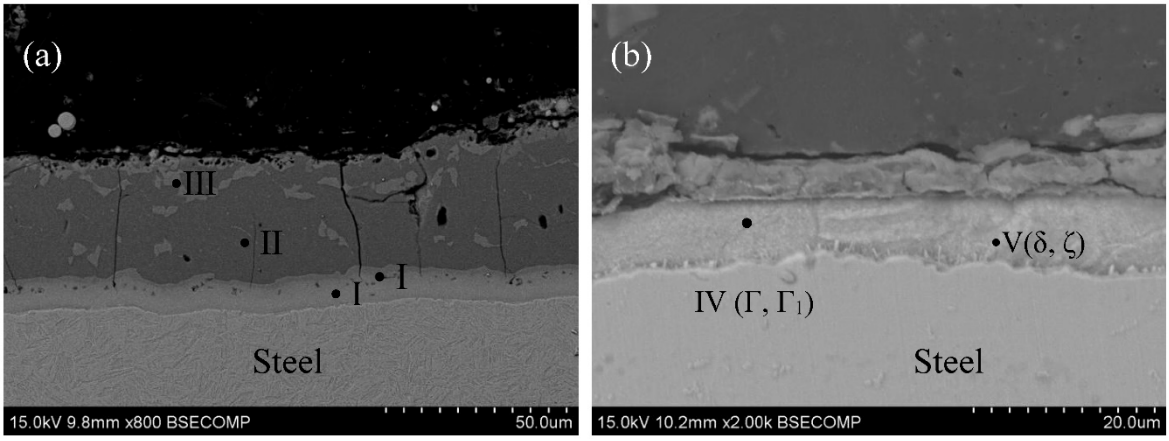

Figure 2. Microstructure of the coatings (a) Al-Si coating and (b) GA coating.

IPG YLS-5000 ytterbium fiber laser was adopted to weld with a lap joint. KUKA six-axis linkage robot was used for experimental automation. The laser wavelength was 1060-1080nm, the minimum focusing spot size was 0.4mm, the beam focal length was 310mm, and the maximum laser power was 6kw. 22MnB5 steel was on the top and galvanized steel was on the bottom. The laser beam is irradiated vertically on the top surface of 22MnB5 steel. The welding speed and laser power are fixed at 2m/min and 3kw. A Variable thickness of Ni foil was put between the 22MnB5 steel and galvanized steel. Figure 3 is a schematic diagram of welding.

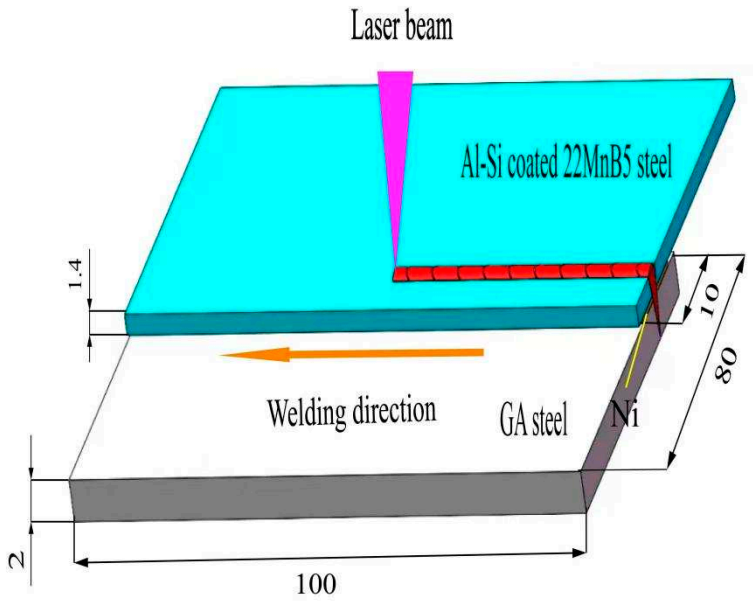

Figure 3. Schematic diagram of laser welding added by Ni foil.

Specimens were cut vertically to the weld for microstructure analysis and strength testing. The dimensions of the tensile shear test specimen are shown in Figure 4. The tensile shear experiments

Preprints (www.preprints.org) | NOT PEER-REVIEWED | Posted: 21 July 2023 doi:10.20944/preprints202307.1453.v1

were carried out at room temperature at a 2 mm/min rate to acquire strength parameters. More than three specimens were used for experiments to obtain an average. In order to observe the microstructure, the specimen for microstructure analysis was polished with coarse and fine sandpaper at first, then polished with a polishing machine, and finally etched by 4% nital solution. The microstructure of the welded joints was analyzed by optical microscope (OM) and scanning electron microscope (SEM) with an energy dispersive spectrometer (EDS). The fracture surface was also analyzed by them. The microhardness was tested using a Micro Vickers at a 100 g load for 10 seconds.

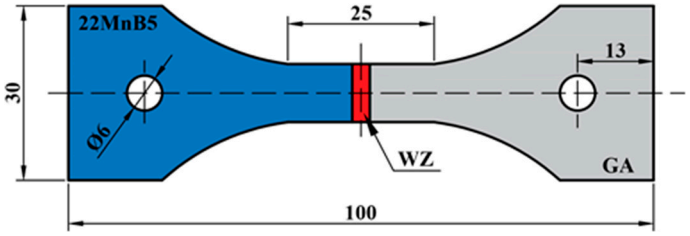

Figure 4. Tensile shear specimen dimensions.

3. Results and discussion

3.1. Weld appearance

With the addition of Ni foil of different thicknesses, the weld profiles of the welded joints are shown in Figure 5. The weld shape was X-shape without Ni foil (No.1) while the weld shape changed into Y-shape with Ni foil (No.2 and 3). After measuring the widths of the welded joints, the top width (B_1) had little change. The cross-section width (B_2) decreased slightly, and the bottom width (B_3) showed a decreasing trend, as shown in Figure 5.

No.	Laser power (kW)	Welding speed (m·min $^{-1}$)	Ni foil thickness (μm)	B_1 (mm)	B_2 (mm)	B_3 (mm)	Cross-section
1	3	2	—	1.61	1.25	1.12	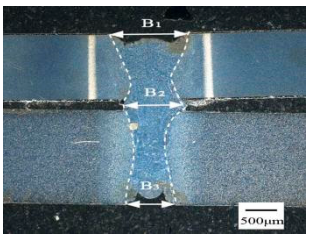
2	3	2	30	1.57	1.03	0.67	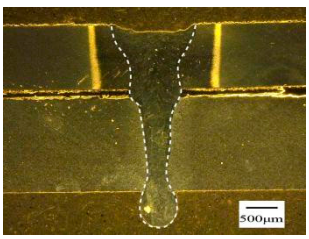
3	3	2	100	1.55	1.08	0.51	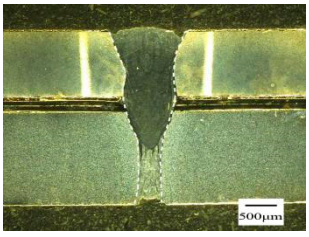

Figure 5. Weld profile and width at different thickness of Ni foil.

Preprints (www.preprints.org) | NOT PEER-REVIEWED | Posted: 21 July 2023 doi:10.20944/preprints202307.1453.v1

The shape and size of the weld are mainly affected by the value of the heat input. When Ni foil was not added, the heat input was large enough, and the depth of the key hole was large. A strong vortex occurred on the upper and lower surfaces of the weld to obtain a completely penetrating weld. Both the top width (B_1) and the bottom bead width (B_3) were wide, so the weld shape is an X-shape. After adding Ni foil at the same heat input, Ni foil would absorb some energy which led to a decrease of heat at the bottom of the weld, therefore, the weld is Y-shaped (No.2 and No.3).

3.2. Microstructure

After laser welding of dissimilar steels, the welded joint can be divided into fusion zone (FZ), heat affected zone (HAZ) and base material(BM). Figure 6 gives the optical images in FZ with 0, 30 and 100μm Ni foil. Without Ni foil, FZ and FB (fusion boundary) comprised a lath-like structure and strip-like white phase (Figure 6 bc). After adding a little of Ni foil (30μm), the amount and size of white phase obviously decreased. At the same time, a new grey phase (FM) appeared. However, no white phases were observed with more thickness of Ni foil(100μm).

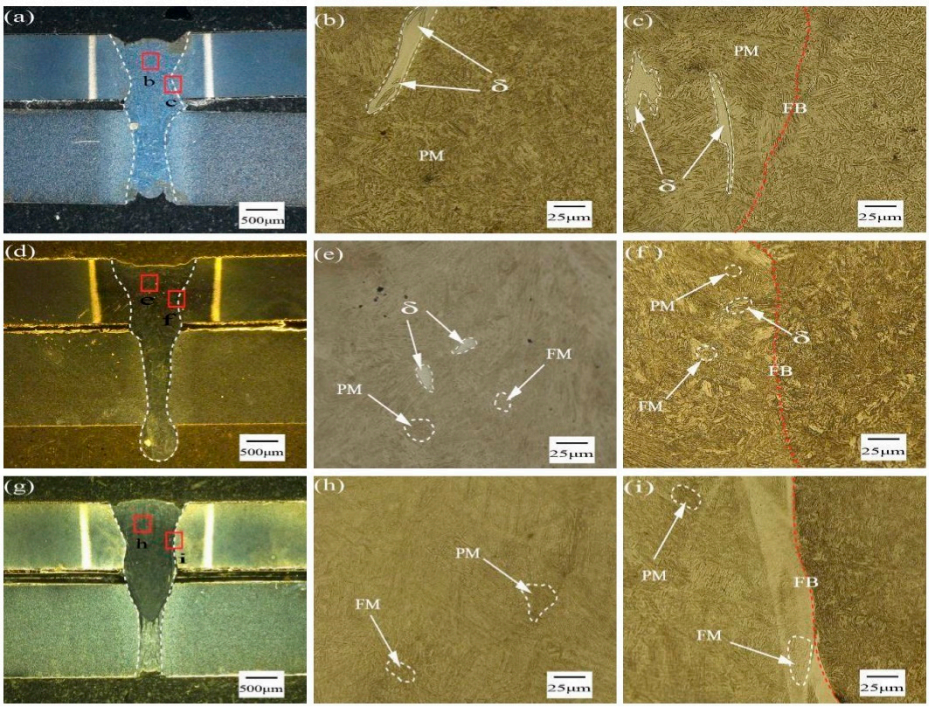

Figure 6. Microstructure of welded joints under different thickness of nickel foil((b:FZ,c:FB,Ni foil not added);(e:FZ,f:FB,30um Ni foil);(h:FZ,i:FB,100um Ni foil)).

To thoroughly analyze the microstructure of the FZ, the SEM and EDS analytical results are given in Figure 7 and Table 2. The color of "white phase" in Figure 6 changed to black color. This was because these phases contained light-weight elements (Al). From the EDS results, P_1,P_2, P_3 and P_4 all contained some Al (7.65%, 6.73%, 3.76%, 3.11%). The same as reference [20], Al element belonged to the ferrite-forming element promoted the formation of δ-ferrite(white band-like). During the laser welding, Al-Si coating was melted into FZ, the gathering of Al in FZ, especially in FB, δ-ferrite phases were formed. However, Zn did not exist in FZ. This was because the boiling point of Zn was very low(903°C). Nearly all of them were vaporized during the welding process. Therefore, little or no Zn existed in FZ after welding.

Preprints (www.preprints.org) | NOT PEER-REVIEWED | Posted: 21 July 2023 doi:10.20944/preprints202307.1453.v1

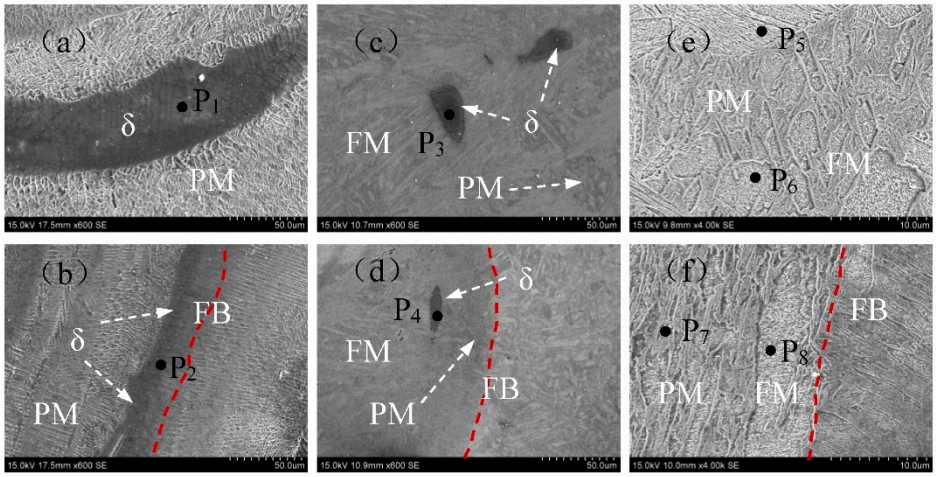

Figure 7. SEM images of weld and fusion boundaries at different Ni foil thicknesses((a:FZ,b:FB,Ni foil not added);(c:FZ,d:FB,30um Ni foil);(e:FZ,f:FB,100um Ni foil)).

Table 2. Chemical composition of different regions(wt. %).

Component /wt.%	P_1	P_2	P_3	P_4	P_5	P_6	P_7	P_8
Al	7.65	6.73	3.76	3.11	0.72	0.63	0.86	0.90
Si	0.98	0.75	0.89	0.54	0.46	0.23	0.31	0.02
Ni	0.12	0.18	2.72	1.40	1.35	4.81	1.42	3.27
Fe	Bal.	Bal.	Bal.	Bal.	Bal.	Bal.	Bal.	Bal.

Except for the "black phases", other phases expressed lath-like. Based on the composition of base material and the quick cooling speed of laser welding, these phases were martensite. But carefully comparing the lath-like phases, they were obviously different. From Figure 6, lath-like martensite was gray without Ni foil. But part of martensite turned greyish-white with 30, especially with 100μm Ni foil, the proportion of greyish-white martensite was very high. From the SEM images of 100μm Ni foil, the size of greyish-white lath (PM) became smaller than gray lath(FM). The EDS results further confirmed that the two martensites were different because the greyish-white lath martensite contained more Ni than grey martensite. Ni element can expand the austenitic phase region which can increase the temperature of A4 and form more γ phases at high temperatures. Since Ni can be infinitely soluble in the γ phase, and the martensite transition temperature (M_S) is reduced, thereby increasing the martensite phase transition hysteresis width ($\Delta T=A_S-M_S$). During cooling, the martensite at high temperatures was called the previous martensite (PM) transition which contained low Ni content. But in high Ni content areas, the Ms point decreased. The martensite transition occurred at low temperatures. This martensite was called Fresh Martensite (FM) transition. The similar phenomenon was observed in reference [21].

The evolution of the microstructure in FZ and FB can be explained as that: During laser welding, both the base material and coatings were melted. Little or No Zn went into the FZ due to its low boiling point. However, Al-Si coating went into the melted welding pool. Al is possibly gathered in FZ, especially at the FB due to the weld pool flow of laser welding (Figure 8ab). Without Ni foil adding the joint, the gathering extent of Al was serious. Al was a ferrite-forming element which promoted the forming of δ-ferrite. Therefore, a large amount of δ-ferrite was formed in FZ, especially big bank-like δ-ferrite were formed due to the hysteresis effect at FB(Figure 9a).

Preprints (www.preprints.org) | NOT PEER-REVIEWED | Posted: 21 July 2023 doi:10.20944/preprints202307.1453.v1

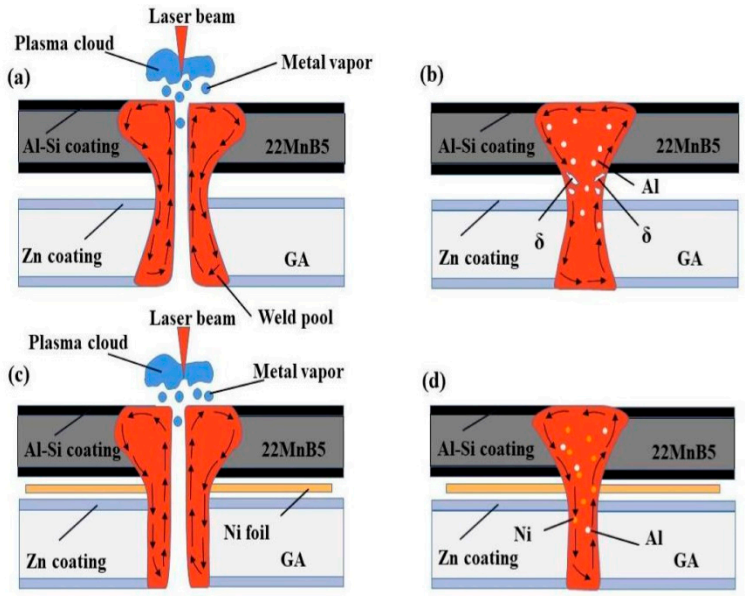

Figure 8. Schematic diagram of weld pool flow((a) (b) Ni foil not added;(c) (d)100um Ni foil).

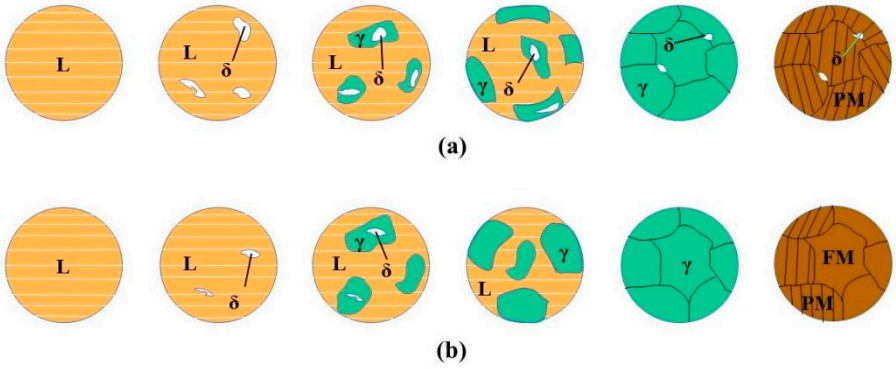

Figure 9. Schematic diagram of tissue phase transition((a):Ni foil not added;(b):100um Ni foil).

After adding Ni foil between the two base materials, Ni was melted into the welding pool(Figure 8b). Since Ni element can expand the austenitic phase region which can inhibit the nucleation and growth of δ-ferrite(Figure 9b). Studies have shown that the same phenomenon is obtained by electron probe microscopy (EPMA), and it can be seen that Ni can well inhibit the macroscopic segregation of δ-Fe caused by the partial polymerization of Al elements [22]. When the amount of Ni was low(30μmNi foil), it was not enough to completely inhibit the macroscopic segregation phenomenon of δ-ferrite caused by Al elements, so a small amount of dot-like δ-Fe was also observed in FZ and FB, as shown in Figure 6ef and Figure 7cd. However, when the amount of Ni exceeded a value (such as 100umNi foil), the δ-Fe phase would disappear.as shown in Figure 6hi and Figure 7ef.

Except for the forming of δ-ferrite, the remained phase featured a lath-like shape microstructure in FZ. This was due to the fact that the cooling speed of laser welding was much faster than the crucial rate of martensitic transition. Initially, generated austenitic would undergo a shear-type phase transition into martensite. As a result, martensite has a lath-like shape in FZ. However, when the joint was added of Ni, Ni could expand the γ phase indefinitely, and formed two different shapes of martensite (PM, FM).The cross-sectional morphology and hardness distribution of HAZ on the side of galvanized steel and 22MnB5 were analyzed with 100μm nickel foil, as shown in Figure 10. The transformation pathways and the resultant microstructure heat-affected zone are given in Table 3. Due to the different base materials and thermal cycles in different positions, the structure of HAZ on the two sides of base materials was different. On the 22MnB5 side, HAZ was separated into a complete quenching zone (UCHAZ), incomplete quenching zone (ICHAZ) and tempering zone (SCHAZ). Among them, according to the grain size, complete quenching zone can be divided into

Preprints (www.preprints.org) | NOT PEER-REVIEWED | Posted: 21 July 2023 doi:10.20944/preprints202307.1453.v1

coarse grain area (CGHAZ) and fine grain area (FGHAZ). Because the peak heating temperature was higher than the austenitic complete transition temperature A_{C3} (CGHAZ and FGHAZ), the martensite first transformed austenitic and subsequently transformed martensite due to the rapid cooling rate(M→γ→M). But the size of grain in CGHAZ was very large due to the high temperature of abnormal grain growth (above 1100℃). So the hardness in the UCHAZ was very high up to 500-550$HV_{0.1}$(Figure 10e). When the temperature was between A_{C3} and A_{C1}(A_{C1}<T<A_{C3}), the incomplete austenitic transformation occurred. The material was heated to the double region. The martensite firstly transformed the two phases: austenitic and α-Fe, then the austenitic transformed martensite (M→γ+α-Fe→M+α-Fe). If the peak temperature of the tempering zone was lower than A_{C1} (T_{temper}<T<A_{C1}), the transformation of tempered martensite occurred(M→TM). Its microhardness was very low(332 $HV_{0.1}$), as shown in Figure 10e.

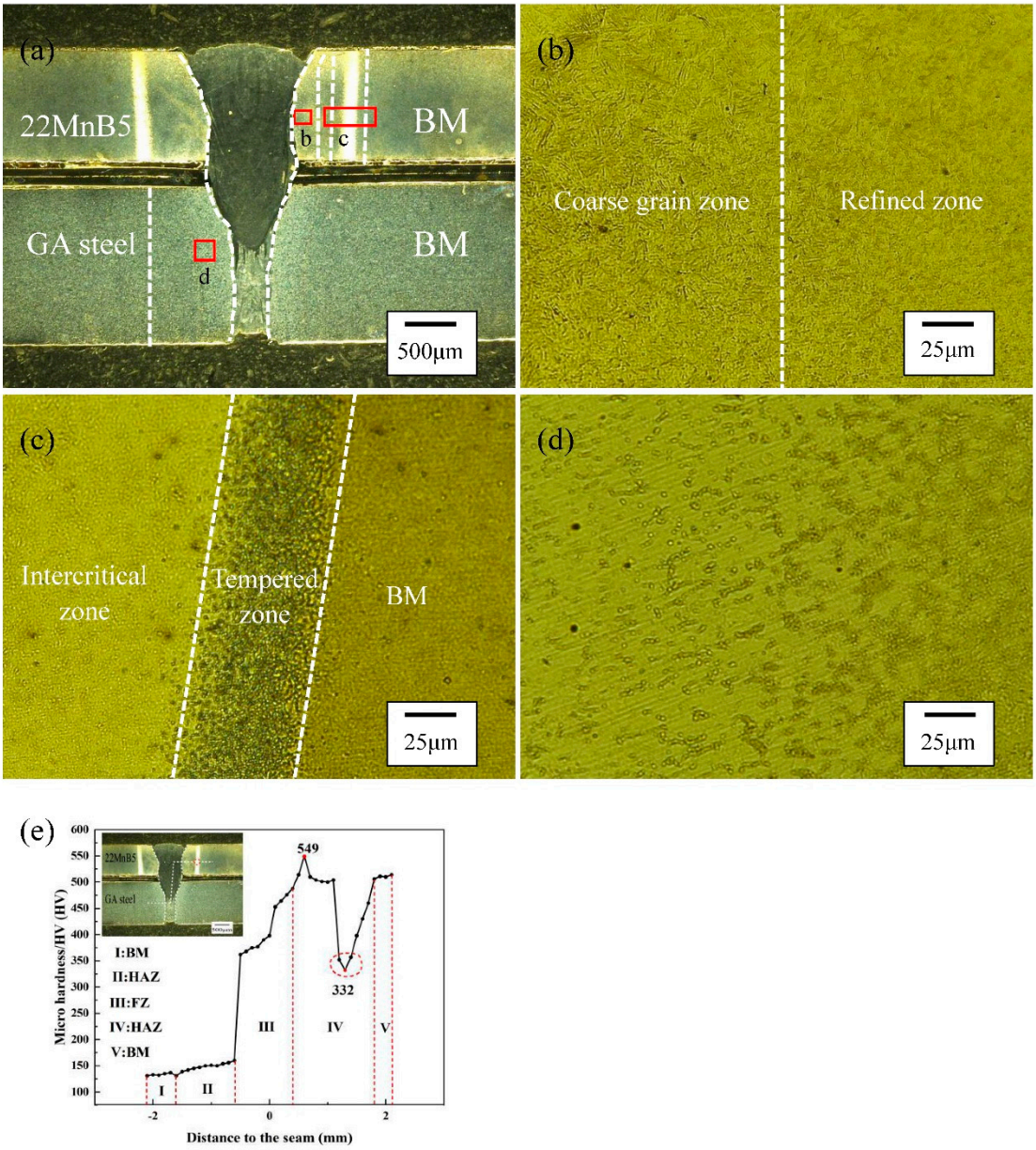

Figure 10. Weld microstructures and hardness profiling (NO.3)(a) over view ; (b) coarse grain zone and refined zone; (c) intercritical zone and tempered zone; (d) HAZ-GA; (e) hardness profile.

Preprints (www.preprints.org) | NOT PEER-REVIEWED | Posted: 21 July 2023 doi:10.20944/preprints202307.1453.v1

Table 3. Summary of transformation pathways and the resultant microstructure in heat-affected zone.

zone		Critical temperature	phase transition process
heat affected zone (22MnB5)	Coarse grain zone	Ac_3<T<1100℃	M→γ→M
	Refined zone	1100℃<T<T_L	
	Incompletely quenched zone	Ac_1<T<Ac_3	M→γ+α-Fe→M+α-Fe
	Tempering zone	T_{temper}<T<Ac_1	M→TM
heat affected zone (GA)	Incompletely recrystallized zone	Ac_1<T	α-Fe+P→γ+α-Fe+P→F+P

On the side of galvanized steel, it is difficult to distinguish different zones due to the quick heating and cooling of laser welding process. The microstructure of BM mainly contained ferrite and very little pearlite. Only part of F+P was transformed austenitic during heating, then recrystallized to the small size of F+P (α-Fe+P→γ+α-Fe+P→F+P). Therefore, only one HAZ-GA was obtained(Incomplete recrystallization zone). As illustrated in Figure 10de, it comprised ferrite and pearlite and displayed very little hardness (150-170 HV0.1).

3.3. Mechanical properties

Table 4 and Figure 11 show the tensile-shear strength and fracture locations of welded joints with variable Ni foil. The tensile strength of the welded joint was deficient without Ni foil, and the fracture location was FB. However, the tensile strength increased with the increasing thickness of Ni foil. The fracture location was from FB changed to interface. The maximum strength can be up to 679MPa under the thickness of 100 μm nickel foil.

Table 4. Tensile strength and fracture location.

NO	Ni foil thickness (μm)	Tensile shear load (N)	Section size B×H(mm^2)	Tensile shear strength (MPa)	Fracture location
0	–	4569	1.1×10	412	FB
1	30	6242	1.2×10	521	FB
2	100	6245	0.92×10	679	Interface

Preprints (www.preprints.org) | NOT PEER-REVIEWED | Posted: 21 July 2023 doi:10.20944/preprints202307.1453.v1

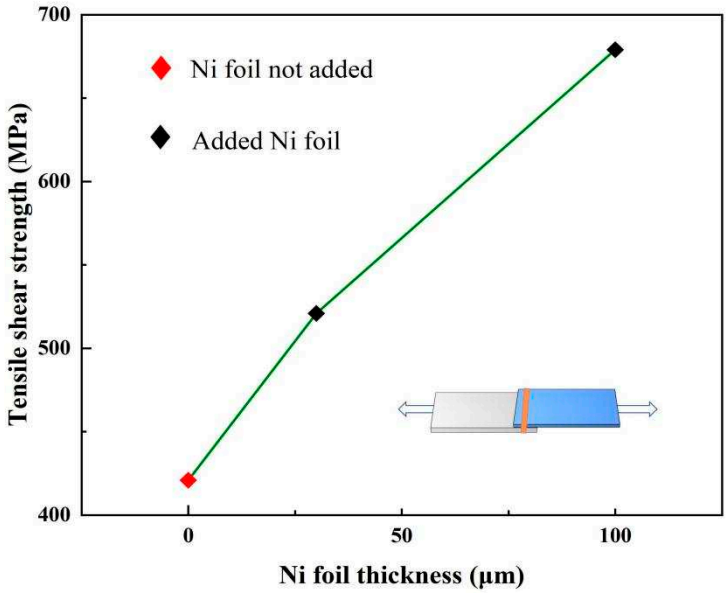

Figure 11. Tensile shear strength at different thicknesses of Ni foil.

Figure 12 and Table 5 give the images and its composition of fracture. In the absence of Ni foil, river patterns (E_1, 8.07 wt.% Al)and big cleavage planes (E_2, 3.05 wt.% Al)were observed. Meanwhile, some dimples also seemed on the fracture surface (E_3, little or no of Al). As a result, the fracture mechanism was a mixture of brittle cleavage, quasi-cleavage, and ductile fracture. It was discovered that the fracture most likely began at the FB near interface with many -ferrite phases and then traveled higher along the FB. That adequately accounted for why the mechanical property of the welded joints without Ni was so low. As added 30μm Ni foil, the cleavage planes were small. Most of the fracture surfaces were dimples. The composition of small cleavage planes also contained Al(E_4, 2.04 wt.% Al). The fracture pattern with 30μm Ni foil mainly contained quasi-cleavage and ductile fracture. Furthering increasing the thickness of Ni(100μm), the fracture surface mainly contained dimples. Compared with the small dimples (E_5, 2.59 wt.% Ni), the big dimples consisted of more Ni(E_6, 8.07 wt.% Ni). The fracture pattern with high Ni was a ductile fracture. All of the above indicated that with no or low amount of Ni, the accumulation of Al at the FB or in the FZ would be harmful to the joint which resulted in low strength due to the low strength and ductility of δ-ferrite(an Al-rich phase). After adding Ni, the amount of δ-ferrite decreased or even disappeared. The strength of the welded joint increased accordingly.

Preprints (www.preprints.org) | NOT PEER-REVIEWED | Posted: 21 July 2023 doi:10.20944/preprints202307.1453.v1

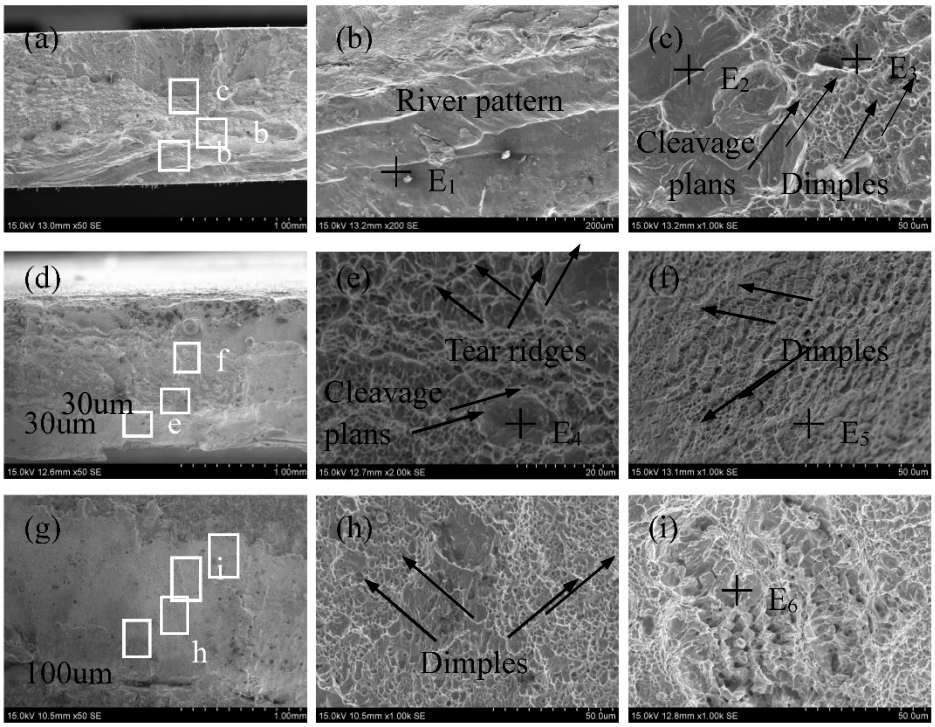

Figure 12. Tensile fracture surface SEM morphologies at various nickel foil thicknesses.

Table 5. Chemical components of the fracture surfaces (wt. %).

Element /wt.%	E_1	E_2	E_3	E_4	E_5	E_6
Al	8.07	3.05	1.12	2.04	1.08	0.30
Si	0.65	0.71	0.52	0.74	0.88	0.16
Ni	—	—	—	1.44	2.59	8.07
Fe	Bal.	Bal.	Bal.	Bal.	Bal.	Bal.

4. Conclusions

After adding Ni foil, the microstructure and mechanical properties of lap laser welding 22MnB5 steel/galvanized steel were discussed in this paper. Based on the results of the experiments, the following conclusions can be drawn:

(1) When Ni foil was not added, the weld appeared X-shape due to enough heat input while the weld turned Y-shape because of the consumption of Ni foil.

(2) With no or a small amount of Ni foil, Al-Si coating melted into the welding pool and formed δ-ferrite (an Al-rich phase with low strength and toughness) in the fusion zone(FZ), especially along the fusion boundary(FB). The amount and size of δ-ferrite phase would decrease with increased Ni foil. With a high amount of Ni foil, δ-ferrite would disappear. Moreover, Except for PM(no or little of Ni), a Ni-rich phase(FM) was obtained in FZ with Ni foil.

(3) Because of the difference between two based materials, HAZs on both sides were obviously variable. On the side of 22MnB5, HAZ had four zones: coarse martensite zone, refined martensite zone, martensite+ferrite zone and tempered martensite zone. HAZ on the galvanized steel side only had one zone: ferrite+ pearlite zone.

(4) After adding Ni foil, the strength of the joint obviously increased. The maximum strength of the joint can be up to 679MP with 100μm nickel foil. The fracture mode contained cleavage brittle, quasi-cleavage and ductile fracture without Ni foil. After adding Ni foil, the toughness of the joint gradually increased, especially adding a high amount of Ni whose fracture mode changed to ductile fracture.

Acknowledgements: The authors sincerely acknowledge the support by Class III Peak Discipline of Shanghai—Materials Science and Engineering (High-Energy Beam Intelligent Processing and Green Manufacturing).

References

1. Hammarberg, S.; Kajberg, J.; Larsson, S. Ultra high strength steel sandwich for lightweight applications. SN Appl. Sci. **2020**, 2, 1040.
2. Zhang, T.L.; Wang, W.G.; Ma, Y.M.; Fang, N.W.; Lin, S.B.; Li, Z.X.; Kou, S. In situ observation of microstructural and inclusions evolution in high-strength steel deposited metals with various rare earth Pr contents. J. Materials **2022**, 15, 1257.
3. Schmitt, J.H.; Iung, T. New Developments of Advanced High-Strength Steels for Automotive Applications. C. R. Phys. **2018**, 19, 641–656.
4. Karbasian, H.; Tekkaya, A.E. A Review on Hot Stamping. J. Mater. Process. Technol. **2010**, 210, 2103–2118.
5. Mori, K.; Ito, D. Prevention of Oxidation in Hot Stamping of Quenchable Steel Sheet by Oxidation Preventive Oil. CIRP. Ann. Manuf. Technol. **2009**, 58, 267–270.
6. Ighodaro, O.L.; Biro, E.; Zhou, Y.N. Comparative Effects of Al-Si and Galvannealed Coatings on the Properties of Resistance SpotWelded Hot Stamping Steel Joints. J. Mater. Process. Technol. **2016**, 236, 64–72.
7. Jia, J.; Yang, S.L.; Ni, W.Y.; Bai, J.Y. Microstructure and Mechanical Properties of fiber Laser Welded Joints of Ultrahigh-Strength Steel 22MnB5 and Dual-Phase Steels. J. Mater. Res. **2014**, 29, 2565–2575.
8. Li, Y.L.; Liu, Y.R.; Yang, J. First Principle Calculations and Mechanical Properties of the Intermetallic Compounds in a Laser Welded Steel/Aluminum Joint. Opt. Laser Technol. **2020**, 122, 105875.
9. Zhou, D.W.; Xu, S.H.; Peng, L.; Liu, J.S. Laser lap Welding Quality of Steel/Aluminum Dissimilar Metal Joint and its Electronic Simulations. Int. J. Adv. Manuf. Technol. **2016**, 86, 2231–2242.
10. Kim, C.; Kang, M.J.; Park, Y.D. Laser welding of Al-Si coated hot stamping steel. Pro. Eng. **2011**, 10 2226–2231.
11. Lin, W.H.; Li, F.; Wu, D.S.; Chen, X.G.; Hua, X.M.; Pan, H. Effect of Al-Si coating on weld microstructure and properties of 22MnB5 steel joints for hot stamping. J. Mater. Eng. Perform. **2017**, 27, 1825–1836.
12. Saha, D.C.; Biro, E.; Gerlich, A.P.; Zhou, Y.N. Fusion zone microstructure evolution of fiber laser welded press hardened steels. Scr. Mater. **2016**, 121, 18–22.
13. Lin, W.H.; Li, F.; Hua, X. Effect of filler wire on laser welded blanks of Al-Si-coated 22MnB5 steel. J. Mater. Process. Technol. **2018**, 259, 195-205.
14. Völkers, S.; Somonov, V.; Böhm, H.C.S. Influence on the Microstructure of Laser Beam Welds of High-strength Steels. J. Lightweight des worldw. **2017**, 10, 40-45.
15. Khan, M.S.; Razmpoosh, M.H.; Macwan, A. Optimizing weld morphology and mechanical properties of laser welded Al-Si coated 22MnB5 by surface application of colloidal graphite. J. Mater. Process. Technol. **2021**, 293, 117093.
16. He, X.; Qin, Y.Q.; Jiang, W.X. Effect of Welding Parameters on Microstructure and Mechanical Properties of Laser Welded Al-Si Coated 22MnB5 hot Stamping Steel. J. Mater. Process. Technol. **2019**, 270, 285–290.
17. Zhang, D.F.; Qin, Y.Q.; Zhao, F.; Liang, M. Microstructure and Mechanical Properties of Laser Welded Al-Si Coated 22MnB5 hot Stamping Steel and Galvanized Steel. J. Mater. Eng. Perform. **2021**, 31, 1346.
18. Razmpoosh, M.H.; Macwan, A.; Biro, E.; Zhou, Y. Microstructure and dynamic tensile characteristics of dissimilar fiber laser welded advanced high strength steels. Mater. Sci. Eng. A-Struct. **2020**, 773, 1-10.
19. Min, S.L.; Moon, J.H.; Kang, C.G. Investigation of formability and surface micro-crack in hot deep drawing by using laser-welded blank of Al–Si and Zn-coated boron steel. J. Eng. Manuf. **2014**, 228, 540–552.
20. Zhao, F.; Qin, Y.Q.; Zhang, D.F. Effect of Filler Wire on Laser Lap Welding of Al-Si Coated 22MnB5 Hot Stamping Steel. J. Mater. Eng. Perform. **2022**, 31, 9670–9680.
21. Yao, Z.; Xu, G.; Jiang, Z. Effects of Ni and Cr on Cryogenic Impact Toughness of Bainite/Martensite Multiphase Steels. Met. Mater. Int. **2019**, 25, 1151–1160.
22. Khan, M.S.; Razmpoosh, M.H.; Biro, E. α-Ferrite Suppression during Fiber Laser Welding of Al-Si Coated 22MnB5 Press-Hardened Steel. Weld. J. **2021**, 100, 213-220.

 doi:10.20944/preprints202307.1453.v1

disclaim responsibility for any injury to people or property resulting from any ideas, methods, instructions or products referred to in the content.